

Solar radiative heating of fiber-optic cables used to monitor temperatures in water

Bethany T. Neilson,¹ Christine E. Hatch,^{2,3} Heng Ban,⁴ and Scott W. Tyler²

Received 3 July 2009; revised 6 April 2010; accepted 19 April 2010; published 25 August 2010.

[1] In recent years, applications of distributed temperature sensing (DTS) have increased in number and diversity. Because fiber-optic cables used for DTS are typically sheathed in dark UV-resistant materials, the question arises as to how shortwave solar radiation penetrating a water column influences the accuracy of absolute DTS-derived temperatures in aquatic applications. To quantify these effects, we completed a modeling effort that accounts for the effects of radiation and convection on a submersed cable to predict when solar heating may be important. Results indicate that for cables installed at shallow depths in clear, low-velocity water bodies, measurable heating of the cable is likely during peak solar radiation. However, at higher velocities, increased turbidity and/or greater depths, the effects of solar heating are immeasurable. A field study illustrated the effects of solar radiation by installing two types of fiber-optic cable at multiple water depths (from 0.05 to 0.8 m) in the center and along the sidewall of a trapezoidal canal. Thermistors were installed at similar depths and shielded from solar radiation to record absolute water temperatures. During peak radiation, thermistor data showed small temperature differences ($\sim 0.003^{\circ}\text{C}$ – 0.04°C) between depths suggesting minor thermal stratification in the canal center. DTS data from cables at these same depths show differences of 0.01°C – 0.17°C . The DTS differences cannot be explained by stratification alone and are likely evidence of additional heating from solar radiation. Sidewall thermistor strings also recorded stratification. However, corresponding DTS data suggested that bed conduction overwhelmed the effects of solar radiation.

Citation: Neilson, B. T., C. E. Hatch, H. Ban, and S. W. Tyler (2010), Solar radiative heating of fiber-optic cables used to monitor temperatures in water, *Water Resour. Res.*, 46, W08540, doi:10.1029/2009WR008354.

1. Introduction

[2] Temperatures recorded at a high spatial and temporal resolution can be used to quantify many fluxes in the hydrologic cycle by using heat as a tracer [Constantz, 2008; Stonestrom and Constantz, 2003]. These fluxes are generally difficult to quantify, in part because variables that control the rates of exchange differ over extremely wide ranges of spatial and temporal scales. While it is possible to deploy point sensors that measure fluxes or temperatures throughout a study area, it can be extremely cost and labor intensive, it may require constant monitoring and replacement of equipment, and it requires separate calibrations and comparisons of individual instruments. By contrast, many distributed temperature sensing (DTS) systems are capable of making accurate temperature measurements at one-meter increments as often as

every 10 s for lengths of up to 5 km [Selker *et al.*, 2006a]. This is higher temporal and spatial resolution than most other methods and requires a single calibration for the entire suite of measurements [Tyler *et al.*, 2009]. For these reasons, DTS applications have become increasingly prevalent in ecological research, and examples abound of its novel contributions to a wide range of processes and environments.

[3] Recent applications of DTS include lake bottom temperatures, mine shaft temperature profiles, glacier air snow interface profiles, lake air water interface temperatures, borehole circulation [Freifeld *et al.*, 2008], snow hydrology [Tyler *et al.*, 2008], soil moisture studies [Sayde *et al.*, 2010; Steele-Dunne *et al.*, 2010], land surface energy exchanges, and temperature distributions along streams [Selker *et al.*, 2006a]. Additionally, these DTS data have been used to quantify groundwater inflows in streams [Selker *et al.*, 2006b], test temperature model predictions [Westhoff *et al.*, 2007], measure snowpack base temperatures [Tyler *et al.*, 2008], and measure the groundwater component of a tidal system on a salt marsh [Moffett *et al.*, 2008]. Many of the current applications in surface water have been conducted in water bodies where the effects of solar radiation may not be a concern (e.g., lake bottoms). However, most water bodies not meeting in-stream temperature standards are commonly partially exposed (unshaded) and have a small depth to surface area ratio. In applications such as these, we seek to quantify the effect of shortwave radiation hitting fiber-optic cables submerged in

¹Utah Water Research Laboratory, Civil and Environmental Engineering, Utah State University, Logan, Utah, USA.

²Department of Geological Sciences and Engineering, University of Nevada, Reno, Reno, Nevada, USA.

³Earth and Planetary Sciences Department, University of California, Santa Cruz, Santa Cruz, California, USA.

⁴Mechanical and Aerospace Engineering, Utah State University, Logan, Utah, USA.

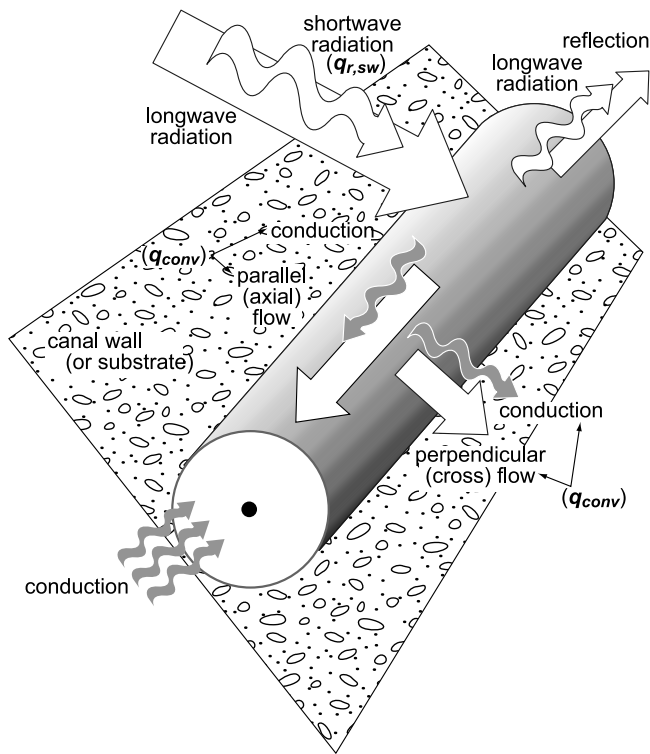


Figure 1. Schematic diagram illustrating the energy balance forces acting on a fiber-optic cable installed in water. Where applicable, specific variable names are included that appear in equations within.

the water on the accuracy of absolute DTS-derived temperatures. The approach of this analysis can be extended from aquatic DTS applications to any fluid-based application using thermal sensors, as all of the issues presented here affect all types of temperature loggers in much the same way.

[4] The shortwave portion of the incoming solar radiation spectrum is typically of concern because it is the dominant process regulating temperatures in many streams [Bowles *et al.*, 1977; Brown, 1969; Brown, 1970; Evans *et al.*, 1998; Sinokrot and Stefan, 1993; Webb and Zhang, 1997]. Furthermore, the greatest penetration of incident solar radiation in water occurs at the shortest wavelengths (72.6% of the radiation between 0.2 and 0.6 μm reaches as deep as 10 m in pure, clear water), and the smallest penetration occurs at longer wavelengths (almost all radiation at wavelengths over 1.2 μm are absorbed in the first few centimeters of water, [e.g., Sellers, 1965]). While the behavior of radiation in water bodies has been studied primarily in lakes and oceans [Austin and Halikas, 1976; Jerlov, 1976; Kirk, 1994; Sweeny *et al.*, 2005], the behavior of photosynthetically active radiation (PAR, which spans the spectral range from 0.4 to 0.7 μm) is commonly measured in streams and other shallow water bodies. However, limited information regarding shortwave radiation (often defined as 0.35 to 1.5 μm , but can range from 0.2 to 4 μm) penetration of freshwater is available [e.g., Dale and Gillespie, 1977; Evans *et al.*, 1998; Johnson, 2004; Kirk, 1994; Sellers, 1965; Wang and Seyed-Yagoobi, 1994; B. T. Neilson, dissertation, 2006].

[5] In DTS and other temperature studies where fiber-optic cables or other temperature sensors are installed in

relatively shallow water, shortwave solar radiation penetrating the water column may cause excess warming and, depending on the intent of the study, could result in erroneous temperature readings. A number of variables influence the amount of radiation penetration and the corresponding potential heating. These include (1) intensity of solar radiation penetrating the water surface as a function of time of day and year, (2) water clarity or vertical attenuation of shortwave radiation (turbidity affects both surface reflection and attenuation of radiation in the water column [e.g., Kirk, 1994; Sellers, 1965; Wang and Seyed-Yagoobi, 1994]), (3) water depth of cable or sensor deployment (solar intensity decreases with depth in the water column), and (4) parallel (axial) and perpendicular (cross) water flow (water movement convects heat away from the cable or sensor). Figure 1 shows a schematic of the potential sources and sinks of heat affecting fiber-optic cables in water, including variables that appear in the equations below, where applicable.

[6] To begin to quantify the effects of solar radiation specifically on fiber-optic cables, energy balance calculations for the cables subjected to various conditions (water velocities, depths, vertical attenuation, and solar intensities) were completed on two fiber-optic cables of different diameter commonly used in DTS applications. To further illustrate the possible effects of solar heating on fiber-optic cables, results are presented from a field study where a DTS system interpreted the signals from two different fiber-optic cables deployed at various constant depths and velocities in a concrete-lined canal.

2. Analytical Methods

[7] To assess the extent of heating of the fiber-optic cable due to penetration of solar radiation, a series of calculations based on an energy balance for the cables was completed for common experimental conditions. The magnitude of external shortwave solar radiation hitting the cable and the convective heat transfer (i.e., heat transferred away from the cable by conduction and water flowing past it) were taken into consideration. Many other heat transfer mechanisms can influence the cables in water (Figure 1), including incoming and back longwave radiation, reflection of longwave or shortwave radiation off the cable, and possibly conduction with any other medium (substrate) that the cable may come in contact with. In these calculations, however, we assume that all shortwave radiation reaching the cable is absorbed by the cable (reflection off cable was insignificant) and that incoming and emitted longwave radiation are negligible heat fluxes in the water. When suspended in the water, the amount of solar radiation hitting the cable per unit area is a function of the intensity of the solar radiation striking and penetrating the water surface, which is, in turn, a function of time of day, water clarity, and water depth. Since the focus of this paper is on the effects of solar radiation on the fiber-optic cables, the influences of the sediments/concrete in which the cable may be in contact with are not considered here. Given these assumptions, a simple energy balance can be written for a unit length of cable (equation (1)).

$$\frac{dE}{dt} = q_{r,sw} - q_{conv} \quad (1)$$

where $\frac{dE}{dt}$ is the change in sensible energy of the cable over time (W), $q_{r,sw}$ is the heat gain due to shortwave radiation per unit length of cable (W), and q_{conv} is the heat loss due to convection per unit length of cable (W).

[8] For a given velocity passing, the convective heat transfer equation (Newton's law of cooling [e.g., *Incropera et al.*, 2007]) can be used to determine the cable heat loss due to convection (equation (2)). Convective heat loss from a unit length of cable is a function of a heat transfer coefficient, the characteristic surface area, and the difference in temperature between the surface of the cable and the bulk fluid (i.e., the flowing water above the cable).

$$q_{conv} = \bar{h}A\Delta T_{SB} \quad (2)$$

where \bar{h} is the average heat transfer coefficient ($\text{Wm}^{-2}\text{K}^{-1}$) over the entire surface, A is the characteristic surface area (m^2), and ΔT_{SB} is the temperature difference between the cable surface and the bulk fluid (K).

[9] The radiative heating (i.e., solar radiation) is equal to the magnitude of the solar radiation striking the cable multiplied by the surface area it is striking (equation (3)).

$$q_{r,sw} = q''_{r,sw} \frac{A}{2} \quad (3)$$

where $q''_{r,sw}$ is the shortwave radiation striking the surface of the cable (Wm^{-2}). In this application, the assumption is made that all radiation reaching the cable is absorbed. Additionally, it was assumed that while the entire surface area of the cable will be influenced by convection, only half of the cable will be uniformly warmed by solar radiation. This assumption is reasonable because of solar radiation intensity being measured by a pyranometer that accounts for the effects of both direct and diffuse radiation.

[10] The energy balance can now be written in terms of equations (2) and (3) as shown in equation (4).

$$\frac{dE}{dt} = q''_{r,sw} \frac{A}{2} - \bar{h}A\Delta T_{SB} \quad (4)$$

In this equation, the time scale of change associated with the forcing information (e.g., shortwave radiation and bulk water temperatures) should be considered. Assuming a 1000 Wm^{-2} change between dawn and solar noon, the incoming shortwave radiation change is approximately 1% every 5 min. The magnitude of changes in water temperature is highly site specific and variable, but these additional changes will be on the order of minutes. For most cables used in aquatic studies, the times necessary to reach thermal equilibrium with the surrounding environment, however, are on the order of seconds. This means that a steady state assumption is appropriate for a given set of forcing conditions and can be used to determine cable heating for these conditions. Therefore, equation (4) can be rewritten to equation (5)

$$0 = \frac{q''_{r,sw}}{2} - \bar{h}\Delta T_{SB} \quad (5)$$

Since we are interested in predicting the amount of warming of the cable due to solar radiation, equation (5) can be solved for ΔT_{SB} (equation (6)) and can provide information

regarding the difference in the temperature at the cable surface and bulk water temperature.

$$\Delta T_{SB} = \frac{q''_{r,sw}}{2\bar{h}} \quad (6)$$

[11] In these equations, the heat transfer coefficient (\bar{h}) (equation (7)) is a function of the thermal conductivity of the water, the Nusselt number, and a characteristic length.

$$\bar{h} = \frac{K}{L} \overline{Nu}_L \quad (7)$$

where \overline{Nu}_L is the average Nusselt number over the characteristic length, L (m), and K is the thermal conductivity of the water ($\text{Wm}^{-1}\text{K}^{-1}$).

[12] The Nusselt number is a function of both the Reynolds and Prandtl numbers and is determined experimentally for different surfaces and flow conditions. The Reynolds number provides for the consideration of the velocity of the water perpendicular the cable (where L is set to the diameter of the cable) or parallel to the cable over a specified cable length (where L is based on expected eddy lengths). For this application, no existing correlations have been found in the literature that estimate the Nusselt number for a very small, long cylinder experiencing both turbulent and/or laminar cross and axial flow. Therefore, a range of heat transfer coefficients resulting from pure cross flow (resulting in a smaller boundary layer and therefore maximizing convective heat transfer) over a cylinder and axial flow along a flat plate (resulting in a larger boundary layer and therefore minimizing convective heat transfer) will be used to bracket the most plausible scenarios encountered in natural systems.

[13] For the cross-flow case, the Hilpert relationship (as referenced in *Incropera et al.* [2007]) was applied (equation (8)).

$$\overline{Nu}_D = C Re_D^m Pr^{1/3} \quad (8)$$

where Re_D is the Reynolds number calculated as a function of the cable diameter (i.e., L is set to D), C and m are constants dependent on the value of Re_D , and Pr is the Prandtl number. In this equation, the constants (C and m) vary with the Re_D and are applicable to Re_D numbers ranging from 0.4 to 400,000. This relationship was established for circular cylinders, but was extended on this application to rectangular shaped cables with rounded edges.

[14] For the axial flow estimate, the Nusselt number approximations were based on a relationship for laminar conditions over an isothermal flat plate (equation (9)) [*Incropera et al.*, 2007].

$$\overline{Nu}_L = 0.664 Re_L^{1/2} Pr^{1/3} \quad (9)$$

where Re_L is the Reynolds number calculated as a function of the characteristic length.

[15] It should be noted that these axial flow calculations are not a function of the cable diameter because the flow is assumed to travel along the cable longitudinally over the characteristic length (L). The characteristic length is the longitudinal distance along the cable that begins at the most upstream point of a boundary layer that is forming. For this reason, the L is assumed to be the same for any shape cable

Table 1. BRUsteel and AFL Telecommunications Cable and Water Thermal Properties

	BRUsteel	AFL	Water
Diameter (m)	0.0038	0.00675 ^a	
Min. Bend Radius (m)	0.076	0.1	
Weight (kg km ⁻¹)	25	39	
Thermal Conductivity (W m ⁻¹ K ⁻¹)	0.3–0.35		0.59
Density (g cm ⁻³)	1.41	1.05–1.1	0.99973
Dynamic Viscosity (N s m ⁻²)			1.23E-03
Kinematic Viscosity (m ² s ⁻¹)			1.04E-06
Heat Capacity (kJ kg ⁻¹ K ⁻¹)			4.189

^aCable cross section is a rounded rectangle with dimensions of 0.005 × 0.0085 m. The diameter here is assumed to be an average of these values.

and will be set within reasonable ranges over which a boundary layer will be allowed to form in natural systems. In these calculations, two characteristic lengths (2 and 20 cm) are assumed to provide a reasonable range of values. Uncertainty with regards to the appropriateness of the \overline{Nu}_L relationship for the cables and the assumed values of L leads to calculations that are much more uncertain than the cross flow calculations. It should also be noted that if the Nusselt numbers were calculated using a relationship for an isothermal plate under turbulent conditions, the predicted ΔT_{SB} values for velocities exceeding 0.1 m s⁻¹ for $L = 2$ cm and 20 cm fall between the predicted values for laminar conditions. Therefore, calculations based on equation (9) are considered to be conservative. Additional information required for the calculations is presented in Table 1.

[16] For any application, an estimate of the intensity of the shortwave radiation hitting the cables ($q''_{r,sw}$) must be determined. Since this is highly site specific, data must be collected in situ using a pyranometer at different depths to yield a spectrally averaged vertical attenuation coefficient (K_d). Broad spectrum light attenuation follows an exponential decay relationship (equation (10)) [Kirk, 1985; Kirk, 1994] analogous to the Beer-Lambert law.

$$E_d(z) = E_d(0)^{-K_d z} \quad (10)$$

where $E_d(z)$ is the downward irradiance at depth z , $E_d(0)$ is the downward irradiance just below the water surface, and K_d is the vertical attenuation coefficient.

[17] Equation (10) can be rewritten so that a plot of $\ln E_d(z)$ (equation (11)) over various depths results in a line with a slope of K_d .

$$\ln E_d(z) = -K_d z + \ln E_d(0). \quad (11)$$

These K_d values are site specific because of the effects of differing suspended and dissolved matter [Kirk, 1985] on the scattering and absorption of the light. Once established for certain conditions, however, these K_d values can be used in equation (10) to predict the amount of radiation reaching specified depths in the water column. It should be noted that the amount of radiation penetrating the water surface (incoming minus reflected) must be known. Figure 2 provides an example of how solar radiation changes throughout the water column given different vertical attenuation coefficients.

3. Site Description

[18] The site chosen for study was a trapezoidal concrete-lined canal that carries water diverted from the Little Bear River directly below Porcupine Dam near Paradise, Utah (Figure 3). The canal has a top width of approximately 2.75 m and a side slope of 1 (45° angle). This section of the canal has a northwest aspect, no riparian shading, and is only partially topographically shaded during the first hour of daylight. Throughout the study period, 24–27 June 2008, water flow and velocity in the canal was stable, but the temperatures of the water being diverted decreased because of a change in the releases from the dam. The turbidity of the water (measured 4.6 km downstream of the diversion) was extremely low (approximated to be 1 to 3 nephelometric turbidity units (NTU)) throughout the study period.

4. Field Methods

[19] The Sensonet Limited[®] Halo[™] DTS (Hertfordshire, United Kingdom) used in this study provides temperature data at 2 m spatial resolution and 1 min temporal resolution (the instrument can sample as often as every 10 s). For this study, we used two standard telecommunications fiber-optic cables with specifications appropriate for DTS. Both cables are composed of central acrylate-coated glass fibers (consisting of a 50 μm diameter glass core surrounded by a 37 μm thick

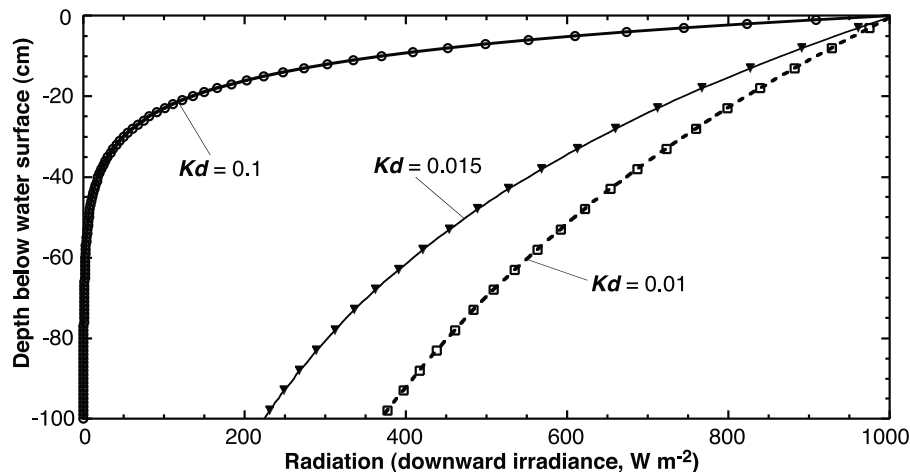


Figure 2. Changes in shortwave radiation/irradiance with depth in the water column given solar input of 1005 W m⁻² at the water surface for three different vertical attenuation coefficients (K_d) in cm⁻¹.

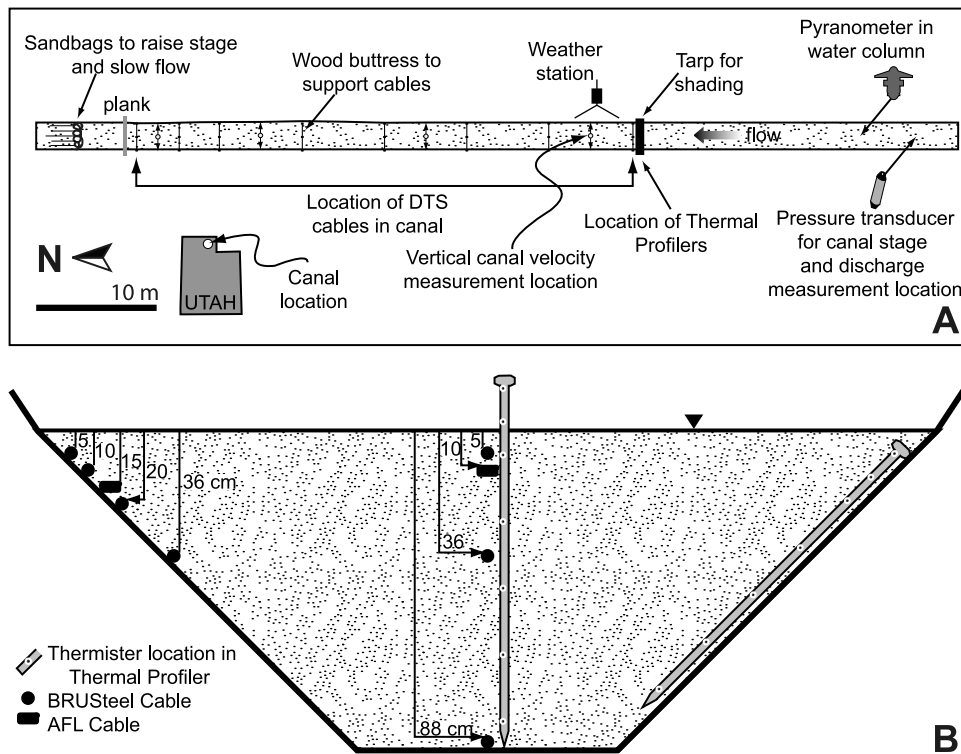


Figure 3. (a) Schematic map and (b) cross section of study location and setup. Figure 3a shows the canal, instrumentation, and measurement locations with an inset showing the site location within the state of Utah. Figure 3b is a cross section approximately corresponding to the “location of thermal profilers” beneath the shade tarp and shows the approximate locations and depths of profilers (shaded) and fiber-optic cables (not shaded) in canal.

glass cladding with a higher index of refraction). Fibers are packed into a gel-filled loose tube and surrounded by strength members and a protective outer jacket. The cables used included a 3.8 mm diameter Brugg Cables, LLC BRUsteel™ cable (Brugg, Switzerland) composed of a steel tube containing four fibers surrounded by steel strength wires and coated with dark blue, UV-resistant plastic, and a 5 × 8 mm diameter AFL Telecommunications, LLC™ All Dielectric Self-Supporting (ADSS) Flat Drop™ cable (AFL is a subsidiary of Fujikura Ltd., Japan) composed of a plastic tube containing two fibers flanked by a fibrous water-blocking material, fiberglass strength rods, and coated with thick black UV-resistant plastic. Note that armoring and strengthening materials represent thirty to sixty times more of the cable volume than the glass fiber itself. As shown in Figure 3, fiber-optic cables were deployed at a number of depths in the center and along the side slope of the canal. Depths and locations in the channel were selected to represent different intensities of solar radiation and water velocities, respectively. At each location (center and side slope), a 40-meter section of fiber-optic cable was strung and attached at several points to maintain the constant, designated depth.

[20] DTS measurements require field calibrations to ensure accurate measurements. Calibration for this experiment involved submersing up to 30 m of the same fiber-optic cable through which measurements were made in a bath of known, constant temperature at each end of the cable. For double-ended measurements, a single calibration bath composed of ice and water yielded a zero-degree constant temperature

offset point (section) correction. For single-ended measurements, one bath provided the offset, and the second bath, at a different, known temperature (in this case, ambient canal water temperature) aided in determination of the slope factor [Tyler *et al.*, 2009]. Calibration baths were refilled with ice and stirred throughout the experiment to maintain constant, zero-degree temperatures. Periodic measurements with a VWR® National Institute of Standards and Technology (NIST) traceable digital thermometer (made by Control Company, with accuracy of 0.05°C) confirmed that ice baths remained at $0.00 \pm 0.05^\circ\text{C}$. Raw DTS data showed apparent changes in ice bath temperatures ranging from $+0.6^\circ\text{C}$ to -0.6°C and represent instrument drift due to changing temperatures of the DTS unit itself and other sources. However, since absolute ice bath temperatures were known to be within $\pm 0.05^\circ\text{C}$ of zero, all DTS data may be corrected for instrument drift by subtracting these apparent excursions. This was achieved by averaging the apparent temperatures over the length of cable submerged in the ice bath for each time, and subtracting that mean value from each temperature along the portion of the cable that was not submerged in the ice bath. This procedure was repeated for each cable at each time. Expected resolution of DTS measurements is indicated by instrument noise floor (or standard deviation) of drift-corrected temperature measurements of the zero-degree bath. For the BRUsteel cable, the 2- σ , or noise level, for spatial (over the ~30 m length of cable in the ice bath) and temporal (over a comparable time period when temperatures were not changing) DTS data are $\pm 0.092^\circ\text{C}$ and $\pm 0.098^\circ\text{C}$, respec-

tively. For the AFL cable, the $2\text{-}\sigma$, or noise level, for spatial (over the ~ 20 m length of cable in the ice bath) and temporal DTS data are $\pm 0.086^\circ\text{C}$ and $\pm 0.096^\circ\text{C}$, respectively.

[21] To support the DTS measurements, thermistor data were collected at 10 cm vertical increments in the center and at 10 cm increments (Figure 3b) along the side slope of the channel at 10 minute intervals in a portion of the canal that was shaded by a tarp (covering approximately 0.5 m of the channel length and was placed about 0.5 m above the water surface) (Figure 3a) to prevent incoming shortwave solar radiation from influencing the instruments or measurements. Thermal profiling probes (Desert Research Institute (DRI), Reno, Nevada) encase seven thermistors each and recorded temperature-time series in the center of the canal at depths of 8, 28, 48, 68, and 86 cm and on the side slope at depths of 2, 9, 16, 30, 44, 59, 73 cm. Throughout the rest of this paper, these data will be referred to as the “reference” thermistors and temperatures because they are not influenced by solar radiation. All reference thermistors were reported by the manufacturer to have $\pm 0.2^\circ\text{C}$ accuracy and resolution of 0.01°C . We conducted a single-point calibration on these thermal profiling probes (thermistors) in a well-mixed reservoir and compared them to a VWR[®] NIST-traceable digital thermometer. The reference thermistors installed in the main channel measured within 0.08°C to 0.11°C of the reservoir temperature and were within $\pm 0.03^\circ\text{C}$ of each other. The reference thermistors installed along the sidewall measured within 0.07°C to 0.12°C of the reservoir temperature, and were within $\pm 0.05^\circ\text{C}$ of each other. On the basis of this calibration, temperature differences of 0.03°C (center) and 0.05°C (sidewall) between thermistors may be resolved at an accuracy of $\pm 0.12^\circ\text{C}$.

[22] With both the DTS and thermistor information, any effects of thermal stratification can be removed in order to assess potential heating on the fiber-optic cable due to solar radiation. Since the reference thermistors measure temperatures in the shade (and represent the actual thermal stratification of the water), these values can be subtracted from temperatures measured by the fiber-optic cables exposed to the sun (representing the combination of the thermal stratification and solar heating). The differences are assumed to be due to the effects of solar radiation on the cable. To complete these calculations, it was necessary to collect various types of supporting data, including variability in water depth (and therefore cable depth) over the study, weather information to document significant changes throughout the study, an estimate of the radiation striking the cables at each depth, and estimates of water velocities moving past each cable.

[23] To ensure consistent cable depths, one-minute water level measurements were taken using a SPXD-610 pressure transducer. Weather data collected included 15-minute shortwave solar radiation, air temperature, and relative humidity on the bank ~ 1.2 m above water surface (Figure 3a). The incoming and reflected solar radiation at the water surface and the attenuation of the shortwave radiation in the water column were measured using an albedometer constructed from two Kipp and Zonen CM3 pyranometers (Bohemia, New York) mounted on a plate with one facing up and one facing down. The spectral range of the instrument ranges from 310 to 2800 nm. Measurements were taken above the water surface (providing a measure of incoming and reflected

radiation) and at four different depths (12, 32, 42, and 62 cm) in the water column at different times during each day of the study to account for any changes in K_d that may have occurred because of changes in water quality (i.e., changes in dissolved or particulate matter due to changes in source water from the dam). In this application, it was assumed that the amount of radiation penetrating the water column was equal to the difference between the observed incoming and reflected radiation above the water surface. The radiation penetrating the water column and the respective attenuation coefficients were used to determine the amount of radiation reaching the depths of interest, as described above.

[24] Local velocities near the surface of the cable were needed in order to quantify the effects of convective heat transfer on the cables for this specific application. Water velocities were measured with a Marsh McBirney Inc.[®] Flo-Mate[™] (Model 2000, Frederick, Maryland) velocity meter. For the cables suspended in the main channel, velocities could be measured at the exact cable depth (Figure 3b), and these data were collected at 4 different locations longitudinally in the study reach (Figure 3a). However, because of the small cable diameter and dimensions of the velocity meter, measurement of the exact velocities near any cables against the concrete surface (i.e., sides slope and main channel bottom cables) was not feasible. In these cases, velocity measurements were taken as close to the cable as possible (~ 4 cm above the cable). Additionally, velocity profiles were measured for the center of the channel and in a vertical profile above each of the cables on the side slope. In order to predict the approximate velocities at the exact cable locations, a log regression was fit to these vertical profiles and extrapolated down to the concrete surface. Velocity profiles were measured on the side slope at four different locations longitudinally throughout the study area (Figure 3a) above each cable at 10, 15, 20, and 36 cm depths. Representative velocities at the cable were established by averaging the measurements taken at different locations.

5. Results

5.1. Analytical Results

[25] Figures 4, 5, and 6 show predictions of the resulting positive ΔT_{SB} (showing cable temperatures in excess of the bulk water temperature) during peak solar conditions at the water surface (1000 W m^{-2}) for both the BRUsteel and AFL cables given different vertical attenuation coefficients, depths, and velocities. To bracket the possible range of ΔT_{SB} values, calculations were completed for both cross flow and axial flow assuming a characteristic length of both 2 and 20 cm. In Figures 4a, 4b, and 4c, plots show that in clear, shallow water (~ 10 cm with a $K_d = 0.01 \text{ cm}^{-1}$) with low velocities, there is a potential for significant warming of the cable for both cross-flow and axial flow cases. For example, in this case, with water flowing at 0.1 m s^{-1} , a BRUsteel cable would measure 0.13°C greater than actual temperatures under pure cross-flow conditions. An AFL cable would measure 0.18°C greater. For a water depth of 50 cm and velocity of 0.1 m s^{-1} , the cross-flow case yields ΔT_{SB} values of 0.09°C and 0.12°C for BRUsteel and AFL cables, respectively. For axial flow at this velocity in 50 cm of water, there could be as much as a 0.53°C warming assuming a 20 cm characteristic length.

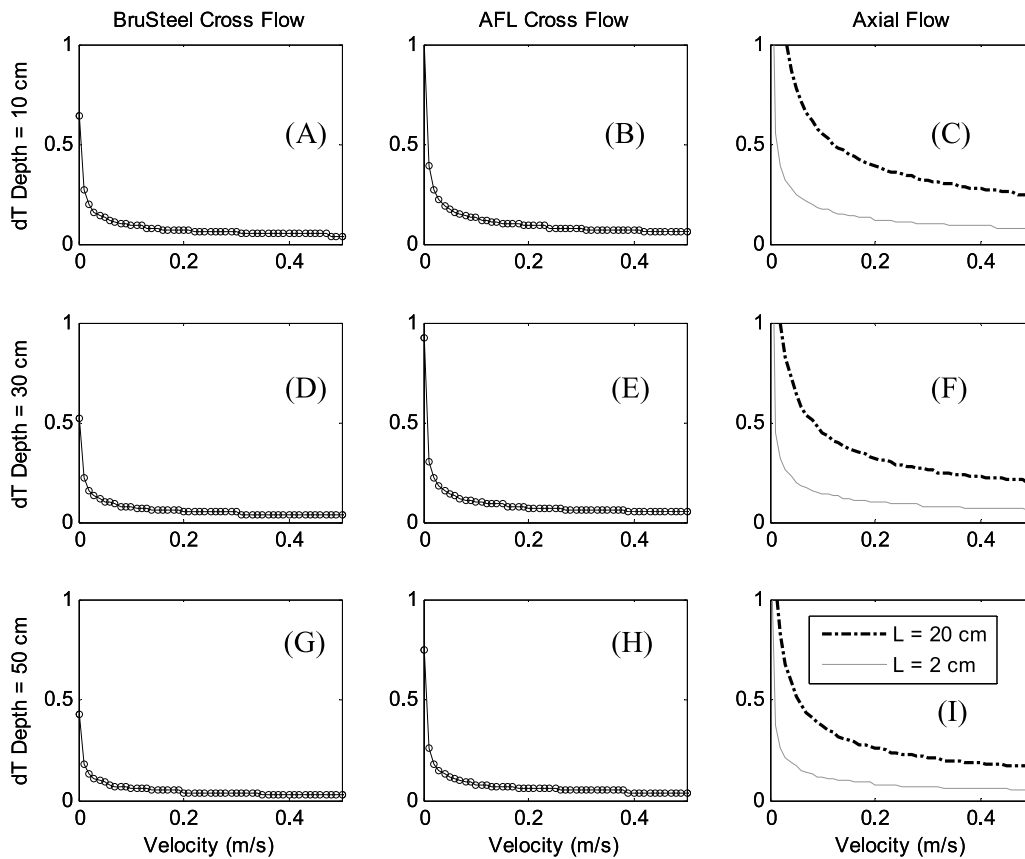


Figure 4. Predictions of heating (ΔT_{SB} , $^{\circ}\text{C}$) on BRUsteel and AFL fiber-optic cables installed under water with a vertical attenuation coefficient (K_d) of 0.01 cm^{-1} (very low turbidity) for (c, f, i) purely axial flow conditions assuming a characteristic length of $L = 2$ and 20 cm and (a, b, d, e, g, h) purely cross flow conditions at water depths of 10 cm (Figures 4a–4c), 30 cm (Figures 4d–4f), and 50 cm (Figures 4g–4i). These calculations assume that 1000 W m^{-2} of shortwave radiation penetrates the air-water interface.

[26] As shown in Figure 5, the potential for heating the cable decreases with a decrease in solar penetration, but in 10 cm of water flowing at 0.1 m s^{-1} , if BRUsteel or AFL fiber-optic cables are exposed to cross-flow conditions where the attenuation coefficient is approximately 0.015 cm^{-1} , they will still experience up to $\Delta T_{SB} = 0.09^{\circ}\text{C}$ and 0.12°C , respectively. The potential for the axial flow ΔT_{SB} is still 0.53°C for a 20 cm characteristic length in 10 cm of water, but decreases to 0.07°C in 50 cm of water. Where there exists a much higher attenuation coefficient ($K_d = 0.1\text{ cm}^{-1}$), warming would be decreased in the cross-flow case to 0.05°C for BRUsteel cable and 0.07°C for AFL cables in 10 cm of 0.1 m s^{-1} velocity water (Figure 6). The ΔT_{SB} under axial flow conditions and high attenuation ($K_d = 0.1\text{ cm}^{-1}$) is 0.32°C in 10 cm of water flowing at 0.1 m s^{-1} for a 20 cm characteristic length. Therefore, even when a fairly large amount of attenuation occurs, enough radiation penetrates the water column to cause concern when water is very shallow.

[27] Given the assumptions made in these calculations, the ΔT_{SB} theoretically increases greatly as the velocity approaches zero. It should be noted, however, that these low velocity predictions are likely inflated because of simplifications in the heat balance used here. While the low velocity predictions are approaching the effect of pure conduction, the calculations do not account for other mitigating factors

(back radiation and, in particular, free convection) that would transfer heat away from the cable as it warms up.

[28] For this study, a key factor in the heat loading to the cables is the shortwave extinction coefficients. The relation between pyranometer-derived extinction coefficients and a more commonly reported measure of turbidity as NTU is not well established and strongly influenced by the nature of the particles leading to adsorption and reflection. However, to provide insight into the attenuation values used within these calculations, recent work (unpublished data) found that using two different colored sediments from the Virgin River, extinction coefficients for turbidities of $30\text{--}90\text{ NTU}$ ranged from 0.025 to 0.065 cm^{-1} , and turbidity values greater than 150 NTU resulted in attenuation coefficients ranging from 0.065 cm^{-1} to values approaching 0.1 cm^{-1} . An attenuation value for tap water was found to be 0.009 cm^{-1} (which should have a turbidity $<5\text{ NTU}$), and distilled, deionized water was found to be 0.0075 cm^{-1} .

5.2. Field Results

[29] The reference thermistors deployed at different depths in the channel showed minor thermal stratification occurring throughout the water column during peak solar hours ($\sim 10:00$ to $14:00$). The relationship between these reference temperatures and water depth was strongly correlated

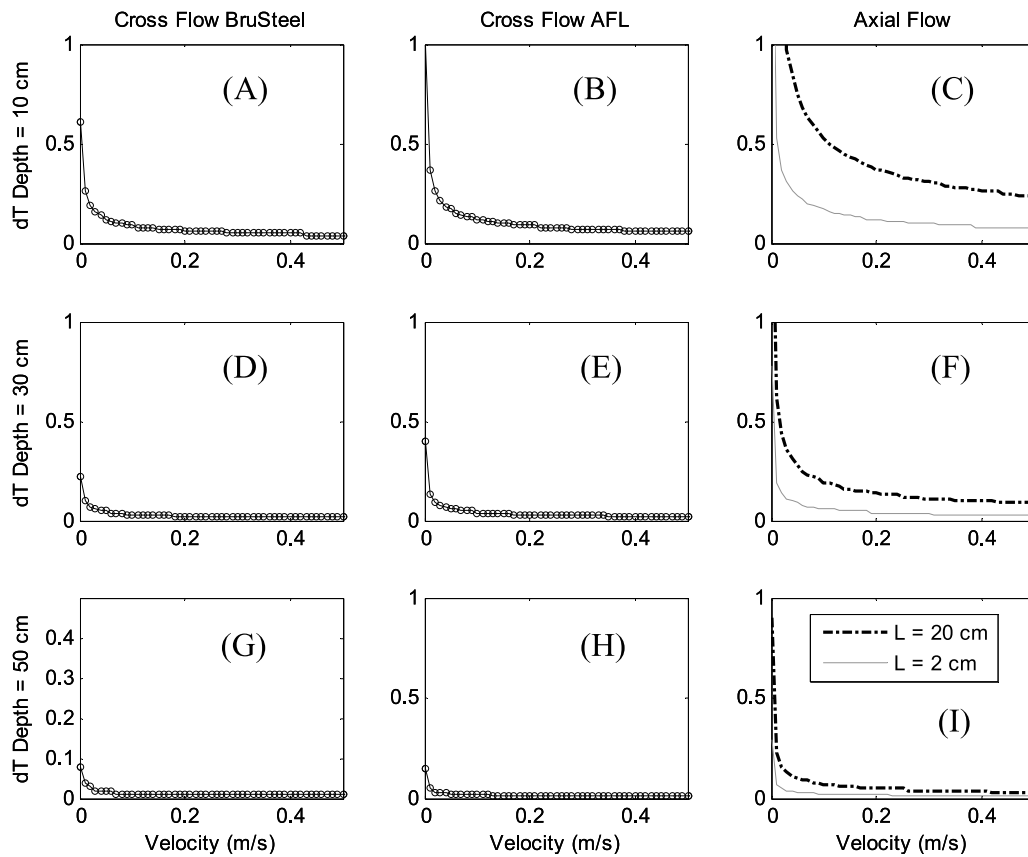


Figure 5. Predictions of heating (ΔT_{SB} , $^{\circ}\text{C}$) on BRUsteel and AFL fiber-optic cables installed under water with a vertical attenuation coefficient (K_d) of 0.015 cm^{-1} (slightly turbid water) for (c, f, i) purely axial flow conditions assuming a characteristic length of $L = 2$ and 20 cm and (a, b, d, e, g, h) purely cross flow conditions at water depths of 10 cm (Figures 5a–5c), 30 cm (Figures 5d–5f), and 50 cm (Figures 5g–5i). These calculations assume that 1000 W m^{-2} of shortwave radiation penetrates the air-water interface.

throughout the study in the upper portion of the water column ($<45\text{ cm}$ on the side slope and $<70\text{ cm}$ in the center of the channel) where the bulk of the fiber-optic cables in the center were deployed. Because of dam-release changes, however, the absolute water column temperatures varied over time. Examples of the reference temperature measurements versus depth at different times and during different days are shown in Figure 7. While the difference in temperatures with depth are much smaller than the instrument accuracy (0.12°C), particularly in the main channel, the relative accuracy ($\pm 0.03^{\circ}\text{C}$ and $\pm 0.05^{\circ}\text{C}$ between thermistors) and resolution of the instruments (0.01°C) allowed us to see consistent trends in the data and suggested thermal stratification in the water column.

[30] Since the reference thermistor locations did not perfectly coincide with DTS cable depths, measured values were interpolated using a linear regression at each time. Interpolated values were resampled at nine-minute intervals (to match frequency of DTS data averages) and are considered to be the reference temperatures at the depth of each cable. As an illustration of the change in temperature with depth and the consistency in the gradient, a subset of the interpolated, or reference, temperatures at the cable depths are shown in Figure 8. Figure 8 highlights the relatively large change in temperature with depth on the side slope during the peak of the day and the smaller differences in the

channel center. During the night, these differences are no longer present in either the side slope or the main channel. This information, together with the fact that these data were collected under the shade of a tarp, suggests that these predictions are representative of the thermal stratification of the water column.

[31] Figure 9 shows single-ended DTS measurements for the same time period from the BRUsteel (solid symbols) and AFL (open symbols) cables at their respective depths. Here individual data points represent an average temperature over the 40-meter length at a specific depth, averaged in time over 9 min. Expected resolution for DTS data based on the variability of drift-corrected ice bath temperatures is twice a single standard deviation of spatial ($\pm 0.046^{\circ}\text{C}$) and temporal ($\pm 0.049^{\circ}\text{C}$) data, respectively. For both cables, spatial variability along each 40-meter section of cable installed at a single depth was very small, averaging 0.05°C and ranging from 0.04°C to 0.09°C . This variability is distributed over the entire 40 m and not concentrated in any section of the cable(s). This random distribution of noise in space indicates that the thermal mixing scales in the canal are longer than the spatial scale of this experiment and are not likely to influence these results. Error bars include one standard deviation for each temperature averaged over 40 m and 9 min (this equals ~ 180 temperatures: 1 per minute every 2 m). DTS data (Figure 9) show the same thermal stratification

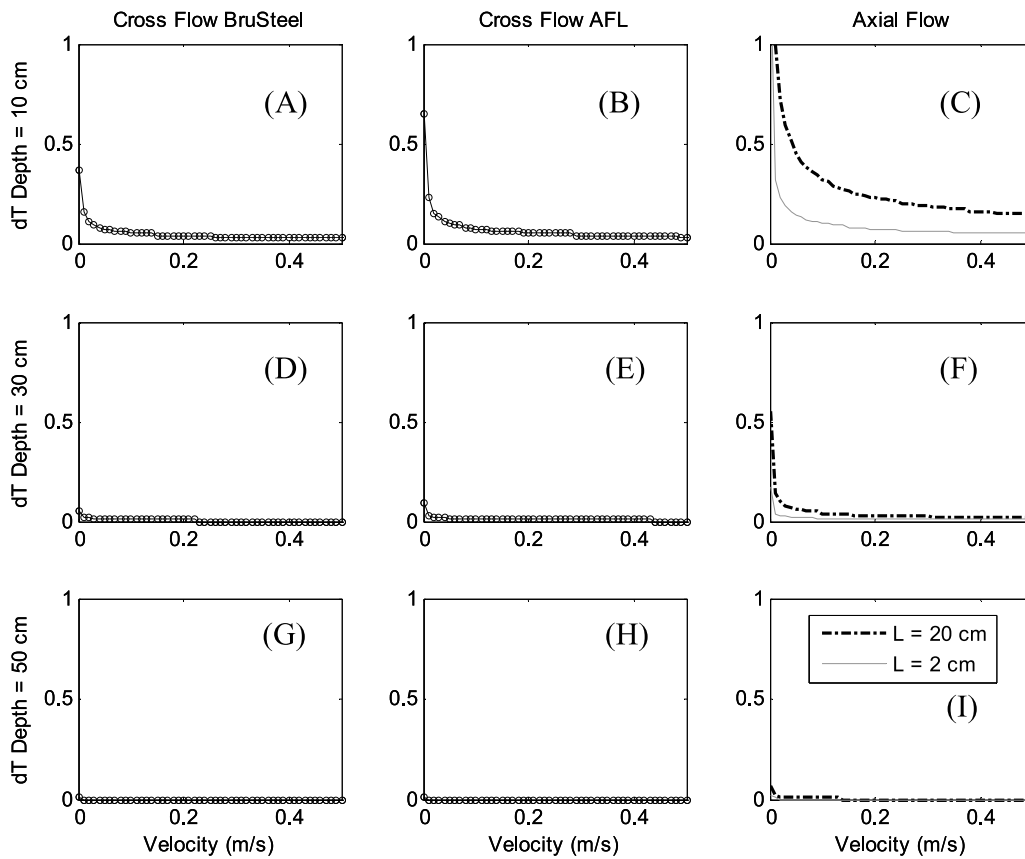


Figure 6. Predictions of heating (ΔT_{SB} , $^{\circ}\text{C}$) on BRUsteel and AFL fiber-optic cables installed under water with a vertical attenuation coefficient (K_d) of 0.1 cm^{-1} (turbid water) for (c, f, i) purely axial flow conditions assuming a characteristic length of $L = 2$ and 20 cm and (a, b, d, e, g, h) purely cross flow conditions at water depths of 10 cm (Figures 6a–6c), 30 cm (Figures 6d–6f), and 50 cm (Figures 6g–6i). These calculations assume that 1000 W m^{-2} of shortwave radiation penetrates the air–water interface.

observed in the reference temperatures (Figure 8), with less separation occurring in the center than along the side slope of the channel during the warmest time of the day. Note that while the AFL cable data exhibit the same general trend as the BRUsteel cable data, they are somewhat warmer than expected. Therefore, the observed differences between BRUsteel and AFL may be due to the larger, darker surface area of the AFL cable absorbing more shortwave radiation.

[32] While the thermal stratification in the water column was recorded by both DTS and the (shaded) reference thermistors, temperature differences with depth measured by the DTS are greater and can therefore provide information regarding potential heating on the unshaded fiber-optic cables. Since reference temperature differences rely on pairs of depths for comparison, only BRUsteel cable was used for the remainder of the discussion, as it was installed at multiple depths on both the sidewall and channel center, while the AFL cable was only installed at a single depth in each location. On the basis of the energy balance calculations, it was anticipated that the cable in the center of the channel would be influenced less by the radiation because of relatively higher velocities resulting in higher convective heat transfer. Lower side slope velocities were expected to yield larger solar influences on the cables.

[33] Figure 10a shows temperature differences between pairs of depths for each measurement technique (e.g., DTS, reference thermistors) for the upper portion of the water column in the center of the channel. The solid line represents the difference between reference temperatures at 5 and 36 cm depths. These data show very little stratification in this portion of the channel. Solid circles represent the temperature differences between DTS measurements at 5 and 36 cm depths and show a diel cycle suggesting that thermal stratification and/or solar heating occurs during peak solar intensity. The positive values illustrate that the cable at 5 cm is warmer than the cable at 36 cm , even though the reference thermistors (in the shade) show that the water temperature at these locations should be nearly the same (Figure 8a and 10a).

[34] In order to determine the portion of the temperature difference that is due to solar heating of the cable for any one pair of depths (i.e., between 5 cm and 36 cm), reference thermistor differences (in the shade) are subtracted from the associated DTS differences (in the sun). We term the result of this subtraction effective solar difference (shown in Figures 10 and 11 as diamonds). The effective solar difference represents the portion of the DTS temperature difference due exclusively to solar radiation and the associated warming of the fiber-optic cable. It additionally represents

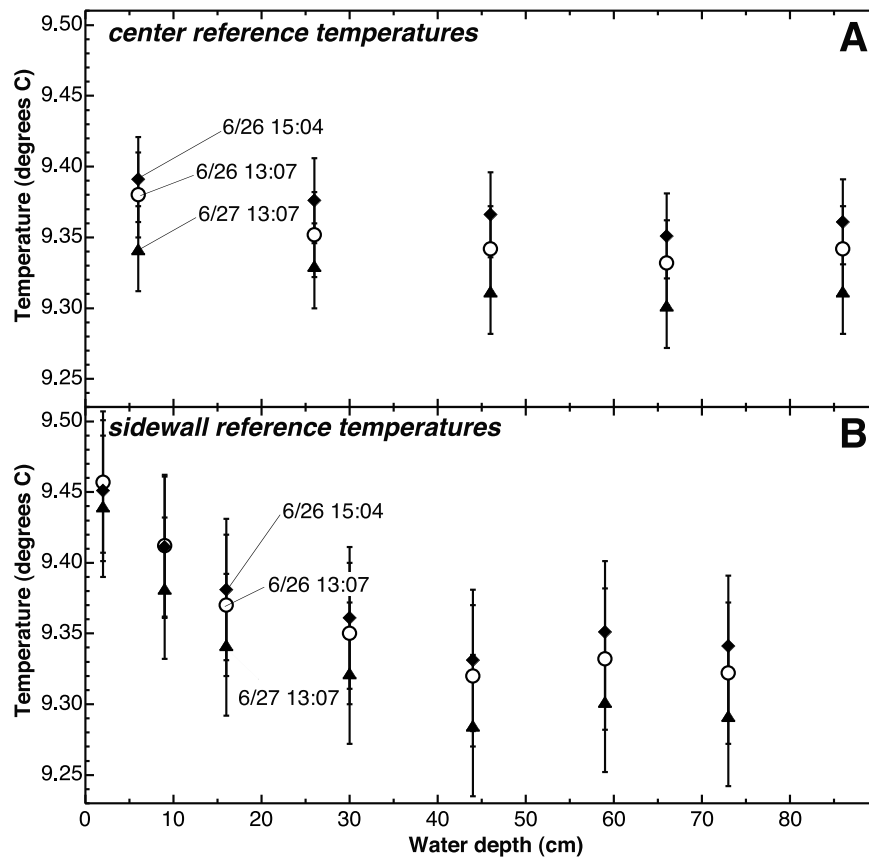


Figure 7. Thermal profiler (DRI, Reno, Nevada) reference thermistor temperatures from different depths in the water column at three different times of day on different days of the study (a) from the center (error bars are $\pm 0.03^\circ\text{C}$) and (b) sidewall (error bars are $\pm 0.05^\circ\text{C}$) of the channel. Minor thermal stratification is most pronounced along the sidewall, but is present in all parts of the channel throughout the study.

the amount of solar heating on the top cable in excess of the heating present on the lower cable and therefore provides an estimate of the amount of heating occurring over this portion of the water column. During the peak solar hours of the day ($\sim 10:00$ – $15:00$), the average effective solar difference between depths of 5 cm and 36 cm in the center of the channel is 0.070°C with maximum and minimum values of 0.093°C and 0.041°C , respectively. During the night, it is anticipated that the effective solar difference should collapse to 0°C . Stratification of the water column may persist and surface heat fluxes between the atmosphere and water (e.g., back radiation) will still be occurring, but there will be no influence of solar radiation on the cable. For this portion of the water column, the average effective solar difference from $\sim 20:30$ to $05:00$ for both nights is 0.008°C , below the resolution of both the DTS and the thermistors.

[35] Figure 10b shows the temperature differences for each measurement technique for the entire water column (5 cm–bottom). The shaded thermistor data here show a temperature difference between 5 cm and the bottom of the channel during the middle of the day. DTS measurements also show a similar thermal stratification, but of greater magnitude. Again, temperatures along the cable at 5 cm are up to $\sim 0.17^\circ\text{C}$ warmer than along the bottom of the channel, suggesting the influence of solar radiation on the cable in shallow water. The effective solar difference (diamonds) during peak solar hours averages $\sim 0.11^\circ\text{C}$ (min = 0.061°C ,

max = 0.149°C). Over the entire water column in the center of the channel, the effective solar difference is 0.013°C during the night. The magnitude of the negative values for the cables increases throughout the night, illustrating that the bottom cable is warmer than the upper cable. While the other cables in the main channel (5 cm and 36 cm) were both suspended in the water column, this bottom cable was in direct contact with the concrete canal bottom which may conduct heat back to the cable during the night. Regardless of the possible additional effects of conduction, the effective solar difference demonstrates that some of the temperature difference measured by the DTS is due to the effects of solar radiation and is in excess of the thermal stratification in the channel.

[36] A feature that is more dominant in Figure 10b than in Figure 10a is the shift in the peak temperature differences recorded by DTS versus the reference thermistors. To explore this phenomenon more thoroughly, we added solar radiation to the plot of the temperature differences (Figure 10b). At sunrise, the initial increase in DTS differences is similar to thermistor differences, however, DTS differences warm two or three times as much as the shaded thermistors as the intensity of the sun increases. The most interesting aspect of these data is the lag in the timing of DTS temperatures decreasing after the sun has set. This suggests that conduction from the concrete bottom continues to heat the water near the concrete after direct solar radiation ceases to do so.

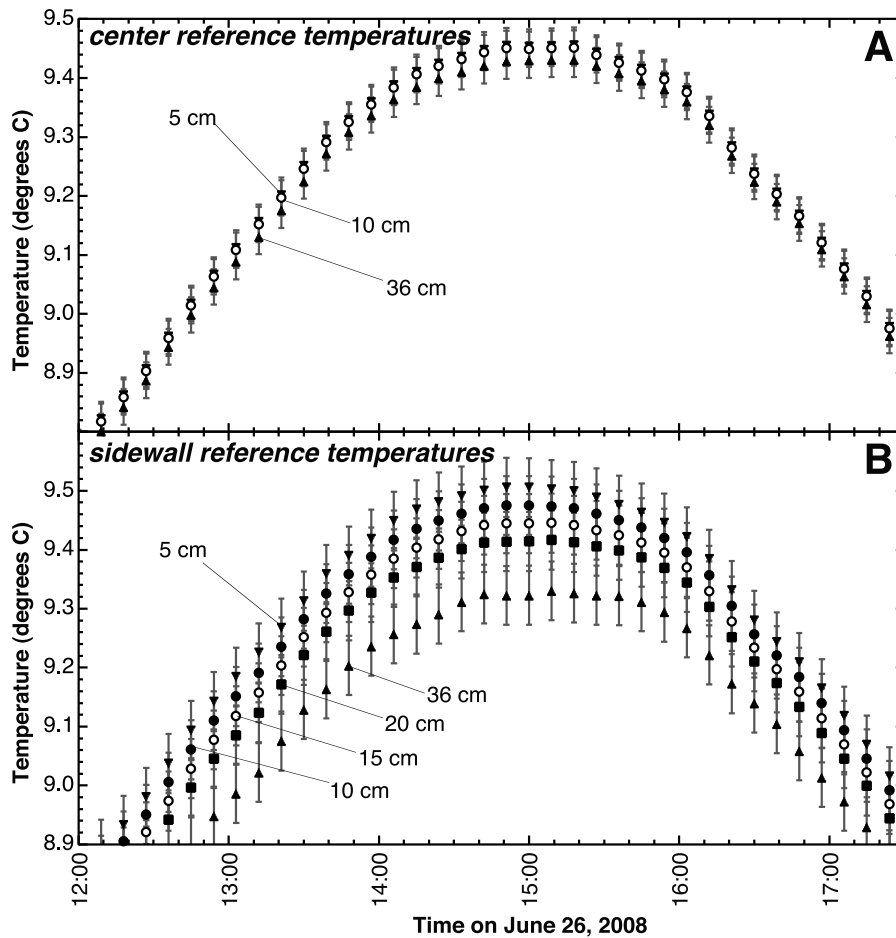


Figure 8. Predictions of reference temperatures at fiber-optic cable installation depths based on the observed linear relationships between water depth and temperature (in Figure 7) at each measurement time. Data shown here at the hottest time of day, from 12:00 to 17:30 on 26 June 2008, illustrate the greatest stratification in (a) the center (error bars are $\pm 0.03^\circ\text{C}$) and on (b) the sidewall (error bars are $\pm 0.05^\circ\text{C}$) of the channel.

Therefore, not only does direct solar radiation on the cable affect the ability to accurately measure water temperatures, but also indirect influences of solar radiation on the substrate affect the ability of the DTS to measure bulk water temperatures due to conduction.

[37] Figure 10c presents the differences between 36 cm and the bottom in the center of the channel. These differences illustrate the diminishing influences of solar radiation in deeper water. Differences from DTS and reference thermistors data are quite similar. During peak solar hours, DTS differences continue to reflect the effects of solar radiation and have an average effective solar difference of 0.039°C (max = 0.066°C , min = -0.004°C). During the night the excess warmth at the bottom of the channel is greater than the stratification measured by the thermistors, again suggesting the influence of conduction from the concrete warming the water at the bottom and therefore the cable.

[38] Figure 11a shows the upper portion of the water column on the side slope of the canal spanning 5 cm and 10 cm. The solid line (thermistor differences) shows that some stratification is occurring at these shallow depths, but none of the values are negative. DTS differences show similar patterns. Effective solar differences (between DTS and ther-

mistors) are often negative, even during the day, demonstrating that the cable at 10 cm is often slightly warmer than the cable at 5 cm. The average effective solar difference during peak solar hours is -0.009°C with a maximum of 0.016°C and a minimum of -0.032°C . These observations suggest that either (1) there is no influence of solar radiation on the cables at this depth, contradictory to what was shown in the main channel, or (2) because of the fact that all of the cables on the side slope are lying against the concrete surface, the influence of conduction from the concrete dampens, or overwhelms, the influence of solar radiation. The time lags in Figure 11b associated with peak temperature differences further support the latter hypothesis. Despite the similar magnitude, the significant time lag between them yields negative effective solar differences averaging -0.012°C (max = 0.032°C , min = -0.060°C) during the day. The effective solar differences for the night average -0.026°C (max = -0.004°C , min = -0.047°C). Negative values indicate that the deeper cable is warmer than the shallower cable.

[39] As mentioned above, timing of peak differences in DTS measurements on the side slope versus the center of the channel is notably different (Figure 11b). Peak DTS differences along the side slope suggest the presence of a heat

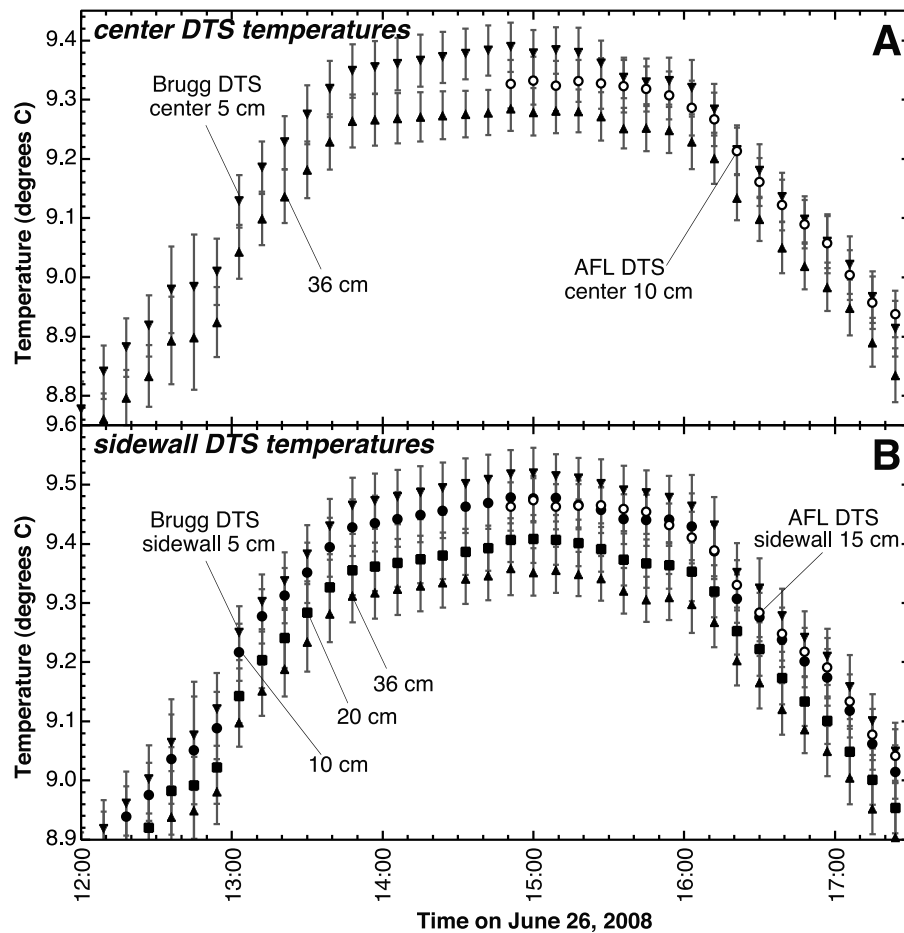


Figure 9. Average distributed temperature sensing (DTS) measurements during peak solar radiation on 26 June 2008 in a trapezoidal canal. BRUsteel (solid symbols) and AFL (open symbols, installed midway through the study) fiber-optic cables are installed at various depths in the center (a) and along the sidewall (b) of the channel. Data were averaged over 40-meter lengths at the same depth, and over 9-minute intervals; error bars are one standard deviation of combined temporal and spatial averaging.

sink that offsets the effects of direct solar influence and a heat source that contributes heat to the cable after peak solar intensity. Contrary to what was found in the channel center between 5 and 36 cm, thermistor data from the side slope (Figure 11c) shows that the stratification of water column alone is greater than the combined effects of solar radiation and stratification measured by the cables. During the day, the cement wall likely absorbs solar radiation and heat from the water because of concrete having a higher thermal conductivity ($1.55 \text{ W m}^{-1} \text{ }^\circ\text{C}$) than water ($0.59 \text{ W m}^{-1} \text{ }^\circ\text{C}$), creating a net energy flux into the wall. As water temperatures cool and solar radiation decreases, the energy flows out of the wall into the water. Because the cable is in direct contact with the wall and/or within the thermal boundary layer near the wall over some significant fraction of its surface area, the DTS measurements represent the effects of this heat source. Both the magnitude and timing of this apparent heat in the side slope DTS data illustrate this phenomenon, especially in contrast to DTS data from the same depths in the center of the channel. All of these observations support the hypothesis that conduction into the cables lying on the concrete influences the ability to measure bulk water temperature outside the boundary layer near the concrete wall accurately. This could additionally be a concern when

placing other temperature sensors on the bed substrate since many sensors (e.g., Hobo Temp Pro V2) have excess material surrounding the measurement device that may be influenced by conduction and affect the accuracy of the temperature measurements.

[40] It should be noted that the variability in the water depth and velocity was relatively small and therefore should not have influenced the differences between DTS temperatures and reference temperatures at various water depths. With the exception of one hour during the middle of the night, the average depth of the water was 0.882 m, with a minimum and maximum of 0.867 m and 0.901 m, respectively. All cable depths were established when the pressure transducer depth was 0.887 m, near the average depth suggesting that on average, the cables were located at the depths specified. Velocity profiles consisted of values ranging between $0.17\text{--}0.84 \text{ m s}^{-1}$ and $0.44\text{--}0.88 \text{ m s}^{-1}$ for the side slope and main channel, respectively.

[41] Using the equations provided earlier, calculations can be completed using information collected during the field study. The K_d values (Table 2) measured throughout the study were found to be consistent. During the peak of the day, 1005 W m^{-2} penetrated the water surface. Using the attenuation coefficient of 0.0151 cm^{-1} , the amount of radia-

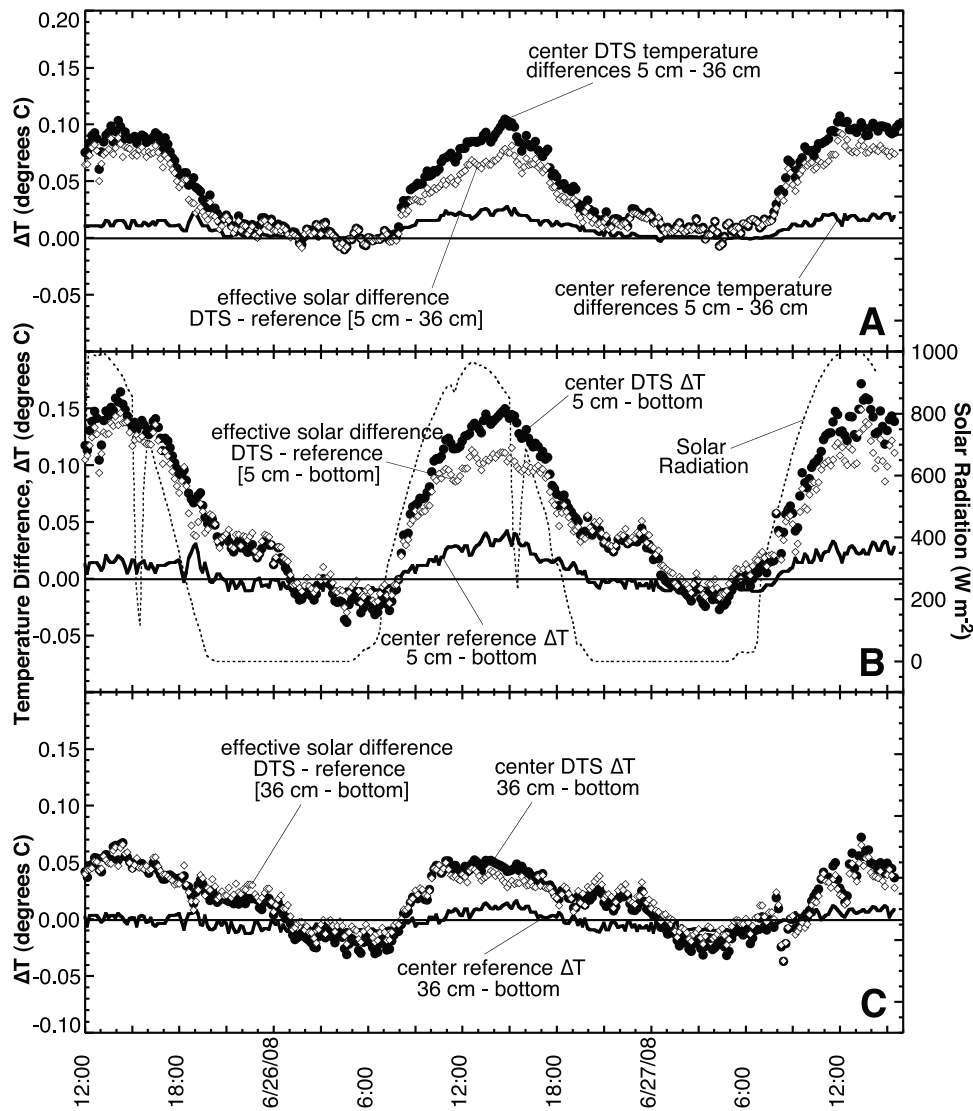


Figure 10. Comparison of channel center temperature differences from pairs of depths (a) 5–36 cm, (b) 5–86 cm (bottom), and (c) 36–86 cm (bottom), measured with reference thermistor strings in the shade (interpolated to same depths as cables, solid black lines) and DTS cables (solid circles) in the sun in the center of the channel. Diamonds represent the effective solar difference, or DTS differences minus thermistor differences. The dashed line in Figure 10b is incoming solar radiation data in $W m^{-2}$.

tion striking each cable can be estimated (Table 3). To estimate the convective heat flux, the velocities either measured or predicted at each cable were necessary (Table 3). The resulting predicted ΔT_{SB} values for each cable type and depth are presented in Table 4. Given the high velocities experienced in this channel, the predicted differences for the BRUsteel cable are small when the cable is experiencing pure cross flow ($0.03^{\circ}C$ – $0.07^{\circ}C$). Assuming axial flow and $L = 2$ cm or 20 cm, the differences become $0.05^{\circ}C$ – $0.13^{\circ}C$ and $0.15^{\circ}C$ – $0.42^{\circ}C$, respectively.

6. Discussion

[42] Using the information from this field effort, a small amount of drift in the DTS data over the course of the experiment complicated direct comparison of reference temperatures to DTS temperatures. However, in an effort to quantify the amount of heating on the fiber-optic cables, we examined

the time-varying offset between reference thermistor data and DTS temperatures at times with maximum (14:00 to 16:00) and minimum (23:00 to 05:00) solar influence. As expected, these calculations result in a smaller average offset at night ($0.55^{\circ}C \pm 0.05^{\circ}C$) than during the day ($0.62^{\circ}C \pm 0.09^{\circ}C$). While not statistically different, these values nevertheless illustrate a qualitative difference between times of solar influence and times without solar influence. They also provide a reasonable measure of maximum heating on the cables because of the influences of solar radiation (Table 5). For the BRUsteel cable, estimated solar heating ranges from $0.01^{\circ}C$ to $0.16^{\circ}C$ at different depths, and for the AFL cable, solar heating ranges from $0.08^{\circ}C$ to $0.17^{\circ}C$. The side slope differences are low because of the effects of conduction on the cables, and an underestimation of any solar heating. Therefore, using the center channel data only, comparisons can be made between the observations (Table 5) and the estimated heating using the assumed cross or axial flow (Table 4). For

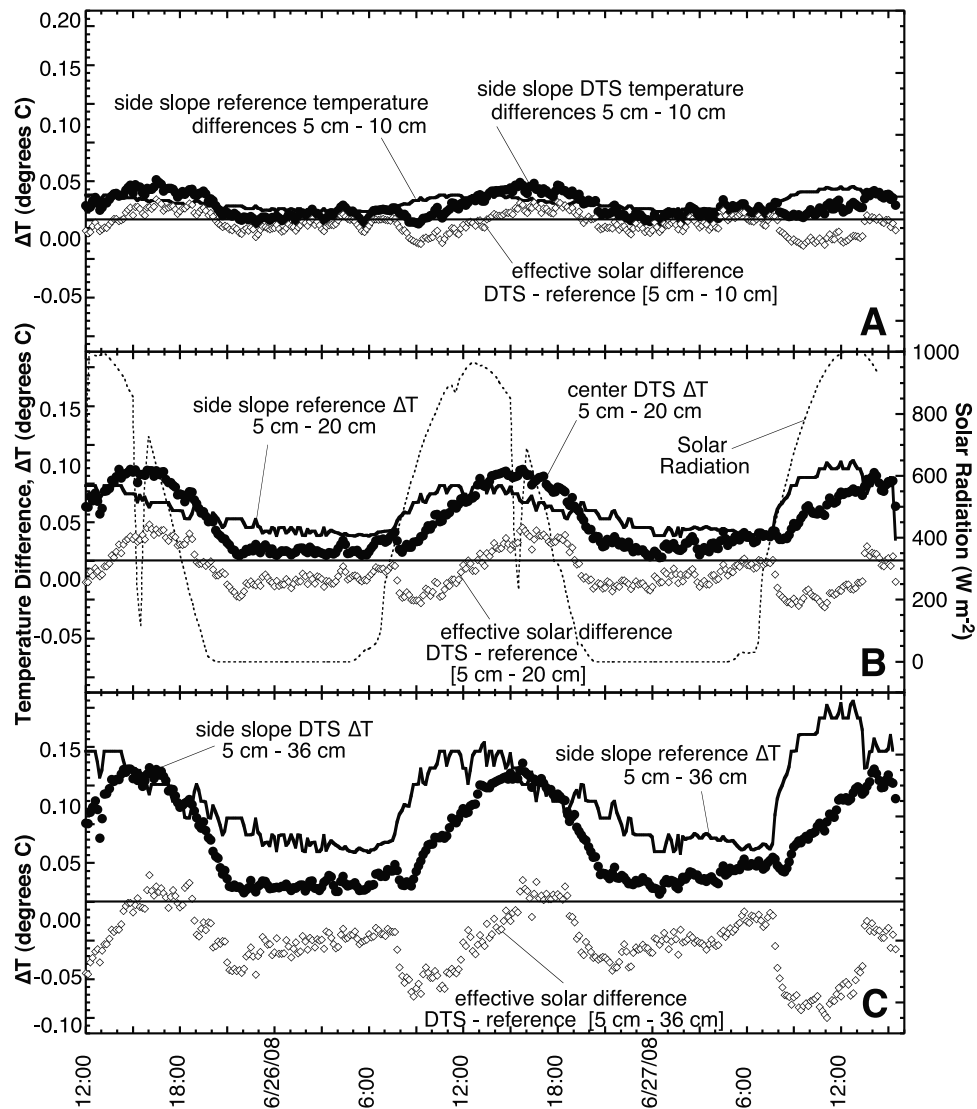


Figure 11. Comparison of side slope temperature differences from pairs of depths (a) 5–10 cm, (b) 5–20 cm and (c) 5–36 cm, measured with reference thermistors in the shade (interpolated to same depths as cables, solid black lines) and DTS cables (solid circles) in the sun on the side slope of the channel. Diamonds represent the effective solar difference, or DTS differences minus thermistor differences. The dashed line in Figure 11b is incoming solar radiation data in W m^{-2} .

the BRUsteel cable at 5 cm, the cross flow calculations (Table 4) predicted similar values to those observed (Table 5). However, at 36 cm depth the observed value lies somewhere between the axial flow calculations, assuming $L = 2$ cm and 20 cm. Similarly, the AFL cable values at 10 cm lie somewhere between the axial flow predictions for $L = 2$ cm and 20 cm. On the basis of the observations, the most appropriate value of L was found to be 7 cm for both the 10 cm AFL cable and the 36 cm BRUsteel cable. It should be noted that these observed differences may not be entirely representative because of the calculations representing the maximum differences over a day (no solar (night) values minus peak solar values). However, they still provide some insight regarding the assumptions of cross or axial flow and they provide consistent information regarding the appropriate characteristic length for the axial flow calculations.

[43] While fiber-optic cable warming due to solar radiation penetration of the water column is something to consider, it is important to note that the magnitude of the warming based on the example calculations and case study presented here highlight some of the conditions that will result in the greatest magnitude of warming. For example, in Figures 4, 5, and 6, these calculations were completed assuming 1000 W m^{-2} penetrates the surface water interface and then attenuates with depth. This is likely the maximum amount of radiation that will penetrate the water surface and will likely only occur during solar noon near the summer solstice (i.e., when the radiation intensity is highest and reflection off the water surface is minimal). To provide a better understanding of the sensitivity of the cable warming to the magnitude of the incoming shortwave radiation, calculations were repeated for a water body that is 10 cm deep with a vertical attenuation coefficient of 0.01 cm^{-1} , and the radiation penetrating the

Table 2. Broad Spectrum Vertical Attenuation Coefficients Estimated at Various Times Throughout the Study

Date	Time	Median Time	Attenuation Coefficients (cm ⁻¹)	R ²
24 Jun 2008	12:47 to 13:12	13:00	0.0131	0.952
24 Jun 2008	15:28 to 15:36	15:32	0.0136	0.956
24 Jun 2008	~16:30	16:30	0.0131	0.969
25 Jun 2008	10:17 to 10:20	10:18	0.0092	0.903
25 Jun 2008	12:45 to 13:08	12:47	0.0151	0.990
25 Jun 2008	14:43 to 14:48	14:45	0.0137	0.984
25 Jun 2008	18:13 to 18:17	18:15	0.0161	0.999
26 Jun 2008	7:58 to 8:03	8:00	0.0175	0.960
26 Jun 2008	10:03 to 10:10	10:06	0.0125	0.961
26 Jun 2008	12:39 to 12:45	12:42	0.0136	0.990
26 Jun 2008	13:45 to 13:49	13:47	0.0142	0.963
26 Jun 2008	15:07 to 15:11	15:09	0.0141	0.996
26 Jun 2008	17:38 to 17:42	17:40	0.0150	0.968
26 Jun 2008	19:05 to 19:10	19:07	0.0143	0.957
27 Jun 2008	8:34 to 8:38	8:36	0.0140	0.980
27 Jun 2008	10:10 to 10:15	10:12	0.0149	0.999
27 Jun 2008	12:02 to 12:07	12:04	0.0140	0.994
27 Jun 2008	13:13 to 13:18	13:15	0.0138	0.987

water surface was reduced to 700 W m⁻² (Table 6). At the lower velocities, the decrease in the cable warming is significantly reduced. For example, assuming cross-flow conditions and using BRUsteel cable in 0.01 m s⁻¹ velocity, 0.12°C less warming would occur if 700 W m⁻² is penetrating this shallow water. An AFL cable would experience 0.16°C less warming. For the axial flow conditions with an $L = 2$ cm, both cables would warm 0.24°C less.

[44] These calculations illustrate that during most times of the day and over a large portion of the year the issues associated with radiation warming the fiber-optic cables are likely immeasurable. Additionally, in many stream systems and other water bodies, shading from riparian vegetation is likely to reduce potential cable heating due to the influence from direct solar radiation. It is also important to reiterate that many of the assumptions made in the simplified energy

Table 3. Measured Velocities and Shortwave Radiation at Water Depths of Each Cable

	Shortwave Radiation Approximated at Cable Depth ^a (W m ⁻²)	Average Velocity at Cable (m s ⁻¹)
Side Slope		
5 cm	932	0.39 ^b
10 cm	864	0.44 ^b
15 cm	801	0.51 ^b
20 cm	743	0.56 ^b
36 cm	584	0.48 ^b /0.33 ^c /0.47 ^d
Main Channel		
5 cm	932	0.77
10 cm	864	0.80
36 cm	584	0.80
88 cm (bottom)	266	0.49 ^b /0.3 ^c /0.87 ^d

^aPredictions are based on a vertical attenuation coefficient of 0.015 cm⁻¹ and 1005 W m⁻² striking the water surface and immeasurable reflection off the water surface. The R² for the vertical attenuation regression was 0.99.

^bThese values were measured ~4 cm above the cable.

^cThese values are velocities predicted at the cable based on a log regression of the velocity distribution directly above the cable.

^dR² values for log regression. The R² values for the side slope are lower because of the influences of the wall on the velocity profiles.

Table 4. Predicted ΔT_{SB} at Fiber-Optic Cable Depths Based on Pure Cross and Pure Axial Flow for BRUsteel and AFL Cables for Field Study^a

Water Depth Above Cable	Predicted ΔT_{SB} Cross Flow		Predicted ΔT_{SB} Axial Flow ^b	
	BRUsteel	AFL	$L = 2$ cm ^c	$L = 20$ cm
Sidewall				
5 cm	0.07	0.10	0.13	0.42
10 cm	0.06	0.09	0.12	0.37
15 cm	0.05	0.07	0.10	0.32
20 cm	0.05	0.07	0.09	0.28
36 cm	0.05	0.07	0.09	0.29
Center				
5 cm	0.05	0.07	0.09	0.30
10 cm	0.05	0.07	0.09	0.27
36 cm	0.03	0.04	0.06	0.18
88 cm (bottom)	0.02	0.03	0.04	0.14

^aTemperature predictions (°C) are based on pure cross flow, or pure axial flow for reference, though real field situations are likely to exhibit a mixture of both.

^bAxial flow predictions are applicable to both cables.

^c L = characteristic length scale for axial flow calculations. This is the length over which a thermal boundary layer will form.

balance results (Figures 4, 5, and 6 and Table 6) produce erroneous estimates of the warming at extremely low velocities because of not incorporating net cooling terms (i.e., free convection and back radiation), which likely become significant in stagnant water. Future efforts to understand the influence of radiation on cables in low-flow environments should be conducted.

[45] One major finding of this study is the need to shield all temperature sensing instruments and to use instruments that have a high reflectivity so as to minimize the effects of radiation within the water column. Even though this study has focused on the effects of solar radiation on DTS cables, similar conclusions can be drawn regarding the impacts of solar heating on other point sensors. Most point sensors,

Table 5. Maximum Estimated ΔT on Fiber-Optic Cables Based on DTS Observations

Water Depth Above Cable	Measured Daily Maximum ΔT ^{a,b}
Sidewall	
5 cm (BRUsteel)	0.01 ± 0.02
10 cm (BRUsteel)	0.02 ± 0.02
15 cm (AFL)	0.08 ± 0.01
20 cm (BRUsteel)	0.04 ± 0.02
36 cm (BRUsteel)	0.02 ± 0.02
Center	
5 cm (BRUsteel)	0.05 ± 0.02
10 cm (AFL)	0.17 ± 0.01
36 cm (BRUsteel)	0.12 ± 0.03
88 cm (bottom, BRUSteel)	0.16 ± 0.03

^aHeating on cables was measured with BRUsteel cable for sidewall depths of 5, 10, 20 and 36 cm, center depths of 5, 36 and 88 cm, and with AFL cable for the sidewall depth of 15 cm and center depth of 10 cm.

^bEstimations for measured heating on cables were made as follows: The average DTS temperature during the day (2 hours of maximum solar influence) was subtracted from the average reference temperature (in the shade) at the same time. Next, the average DTS temperature during the night (no solar influence) was subtracted from the average reference temperature at the same time (this value represents the amount DTS temperatures are offset from the reference). The difference between the offset from reference temperatures during the day (solar influence) and night (no solar influence) indicates the estimated heating on each fiber-optic cable at each depth.

Table 6. Estimates of ΔT for BRUsteel and AFL Cables Under Cross and Axial Flow Conditions^a

Velocity m s^{-1}	BRUsteel Cross		AFL Cross		Axial ($L = 2 \text{ cm}$)	
	$\Delta T_{\text{SB}} 700 \text{ W m}^{-2}$	$\Delta T_{\text{SB}} 1000 \text{ W m}^{-2}$	$\Delta T_{\text{SB}} 700 \text{ W m}^{-2}$	$\Delta T_{\text{SB}} 1000 \text{ W m}^{-2}$	$\Delta T_{\text{SB}} 700 \text{ W m}^{-2}$	$\Delta T_{\text{SB}} 1000 \text{ W m}^{-2}$
0.01	0.27	0.39	0.39	0.55	0.55	0.79
0.1	0.09	0.13	0.13	0.18	0.17	0.25
0.2	0.07	0.10	0.09	0.13	0.12	0.18
0.3	0.06	0.08	0.08	0.11	0.10	0.14
0.4	0.05	0.07	0.07	0.09	0.09	0.12
0.5	0.04	0.06	0.06	0.09	0.08	0.11

^aConditions for 700 and 1000 W m^{-2} penetrating the air-water interface for 10 cm of water assuming a vertical attenuation coefficient (K_d) of 0.01 cm^{-1} .

such as those used in this study, have cross-sectional areas similar to or perhaps larger than the DTS cable used in this study, and are also generally manufactured of materials that will absorb significant shortwave radiation. As a result, these instruments are also likely to suffer similar impacts of solar radiation as DTS cables. Unlike DTS cables, which allow integration of temperature signals over 1–2 meters of length, point samplers such as thermistors may show greater variability in temperature because of either small-scale shading or spatial variations in the thermal boundary layer at the bottom of the stream. While these effects are generally small for either point sensors or DTS cables, care must be taken under conditions of clear and slow-flowing waters for many of the thermal sensing systems.

[46] While it is beyond the scope of this study, it is important to note the potential effects of the heat exchanges with bed sediments on DTS measurements, and to further study these influences in the future. For example, advective heat transport from discharge of hyporheic flow and bed conduction may be significant and were not included here. In this study, the effect of the uniform, flat concrete bed on the cables was notable. The influence of bed substrate on DTS measurements in natural systems, however, will vary because of substrate roughness (yielding much less direct contact between cable and bed materials) and the hydraulic and thermal conductivity of the sediments. When using DTS systems in natural channels that have variable substrate sizes, the cable is typically suspended in the water with occasional points of contact with the bed. Additionally, the temperature measurements are integrated over 1–2 meters and the influences of bed conduction on these integrated temperature measurements may be much less significant. Depending on the placement of other types of temperature sensors, point measurements may also be predisposed to measure the effects of sediment heat fluxes.

7. Conclusions

[47] In this study, four factors were found to affect the temperature of fiber-optic cables and thus our ability to make accurate DTS measurements: penetration of solar radiation, water velocity, water depth, and bed conduction. The focus of the study was on determining the effects of peak solar radiation on fiber-optic cables under typical conditions found in streams (that may also be extrapolated to other environments) and included various velocities ($<1 \text{ m s}^{-1}$) and depths ($<1 \text{ m}$). A simple energy balance was completed for the fiber-optic cables that included the effects of solar heating and convective heat transfer. Since no correlations were found to estimate heat transfer coefficients for a very small, long cylinder experiencing both turbulent and/or laminar cross and axial

flow, both pure cross flow over a cylinder and axial flow along a flat plate were used to bracket the most plausible scenarios encountered in natural systems. However, the question of an appropriate characteristic length resulted in more uncertainty in the axial flow calculations.

[48] Predictions of cable heating illustrated that both BRUsteel and AFL cables will warm significantly under high solar radiation penetration (low vertical attenuation coefficients), low water depths, and low velocities. Cross-flow calculations illustrated that AFL cables will warm more than BRUsteel cables because of a larger surface area. Axial flow calculations did not consider the effects of the cable diameter and therefore could not differentiate between warming of the BRUsteel and AFL cables. Under pure cross-flow conditions for BRUsteel cables and low vertical attenuation values (0.01 cm^{-1}), the predicted ΔT_{SB} values were found to exceed 0.1°C given depths of 10 cm , 30 cm , and 50 cm at velocities less than 0.21 m s^{-1} , 0.14 m s^{-1} , and 0.08 m s^{-1} , respectively. For AFL cables experiencing cross-flow conditions and low vertical attenuation values (0.01 cm^{-1}), the predicted ΔT_{SB} values exceed 0.1°C given depths of 10 cm , 30 cm , and 50 cm at velocities less than 0.32 m s^{-1} , 0.26 m s^{-1} , and 0.17 m s^{-1} , respectively. For both cables experiencing axial flow conditions ($L = 2 \text{ cm}$) and low vertical attenuation (0.01 cm^{-1}), the predicted ΔT_{SB} values exceeded 0.1°C for depths of 10 cm , 30 cm , and 50 cm at velocities less than 0.57 m s^{-1} , 0.47 m s^{-1} , and 0.32 m s^{-1} , respectively. If field conditions exist that are likely to produce excess heating on fiber-optic cables, nighttime measurements may be more reliable (but may still be influenced by bed conduction). In environments where there exist higher velocities, shading of the water body of interest by vegetation, increased vertical attenuation of solar radiation, and/or greater water depths, the effects of solar heating on both cables will become immeasurable.

[49] Field results illustrated the effects of solar warming in a canal with velocities near the cables ranging from 0.3 to 0.8 m s^{-1} . During peak solar conditions during the summer, two types of fiber-optic cable were installed at multiple water depths (from 0.05 to 0.8 m) in the center and along the sidewall of the trapezoidal canal. Thermistors were installed at similar depths and shielded from solar radiation to record absolute water temperatures. During peak radiation, thermistor data showed small temperature differences between depths ($\sim 0.003^\circ\text{C}$ – 0.04°C) suggesting minor thermal stratification in the canal center. DTS data from cables at these same depths show differences of ($\sim 0.01^\circ\text{C}$ – 0.17°C). Observations of these differences suggested that while the cross-flow calculations may be appropriate in some circumstances, the axial flow calculations (with an assumed characteristic length of 7 cm) were also found to be appropriate. For the cables in

contact with the concrete walls, bed conduction appears to be influencing the ability to measure bulk water column temperatures accurately.

[50] These predictions and observations suggest there are many combinations of water clarity, velocities, and water depths (particularly in clear, low velocity shallow water) where care should be taken in the experimental design and DTS data interpretation. Additionally, it is anticipated that the influences of solar radiation should be a concern for all temperature sensors, and the findings of this investigation may be extended to studies using thermal sensors of any kind in aquatic environments.

[51] **Acknowledgments.** We would like to thank our field crew including Quin Bingham, Noah Schmadel, Jon Bingham, Andrew Hobson, and Andrew Neilson for countless hours spent setting up, maintaining, and taking down the experiment. We would also like to acknowledge John Selker for his pioneering research with DTS and his willingness to share that knowledge with us and the larger scientific community. Additionally, Steve Chapra provided much insight regarding various aspects of the study. We would like to thank the Utah Water Research Laboratory, U.S. Bureau of Reclamation agreement 06FC204044, and National Science Foundation Grant EAR-0929638 for partial support of this research. Finally, we appreciate the insightful commentary from Fred Day-Lewis, Jim Constantz, and two anonymous reviewers that significantly improved this paper.

References

- Austin, R. W., and G. Halikas (1976), The index of refraction of seawater, *SIO Ref. 76-1*, Univ. of Calif., San Diego Visibility Lab. of the Scripps Inst. of Oceanogr., San Diego.
- Bowles, D. S., D. L. Fread, and W. J. Grenney (1977), Coupled dynamic streamflow-temperature models, *J. Hydraul. Div., Am. Soc. Civ. Eng.*, 103(HY5), 515–530.
- Brown, G. W. (1969), Predicting temperatures of small streams, *Water Resour. Res.*, 5(1), 68–75.
- Brown, G. W. (1970), Predicting the effect of clearcutting on stream temperature, *Journal Soil Water Conserv.*, 25, 11–13.
- Constantz, J. (2008), Heat as a tracer to determine streambed water exchanges, *Water Resour. Res.*, 44, W00D10, doi:10.1029/2008WR006996.
- Dale, H. M., and T. Gillespie (1977), Diurnal fluctuations of temperature near the bottom of shallow water bodies as affected by solar radiation, bottom color and water circulation, *Hydrobiologia*, 55(1), 87.
- Evans, E. C., G. R. McGregor, and G. E. Petts (1998), River energy budgets with special reference to river bed processes, *Hydrol. Processes*, 12, 575–595.
- Freifeld, B. M., S. Finsterle, T. C. Onstott, P. Toole, and L. M. Pratt (2008), Ground surface temperature reconstructions: Using in situ estimates for thermal conductivity acquired with a fiber-optic distributed thermal perturbation sensor, *Geophys. Res. Lett.*, 35, L14309, doi:10.1029/2008GL034762.
- Incropera, F. P., D. P. Dewitt, T. L. Bergman, and A. S. Lavine (2007), *Fundamentals of Heat and Mass Transfer*, John Wiley, Hoboken, N. J.
- Jerlov, N. G. (1976), *Marine Optics*, Elsevier Sci., Amsterdam.
- Johnson, S. L. (2004), Factors influencing stream temperature in small streams: Substrate effects and a shading experiment, *Can. J. Fish. Aquat. Sci.*, 61, 913–923.
- Kirk, J. T. O. (1985), Effects of suspended solids (turbidity) on penetration of solar radiation in aquatic systems, *Hydrobiologia*, 125, 195–208.
- Kirk, J. T. O. (1994), *Light and Photosynthesis in Aquatic Systems*, Cambridge Univ. Press, U.K.
- Moffett, K. B., S. W. Tyler, T. Torgersen, M. Menon, J. S. Selker, and S. M. Gorelick (2008), Processes controlling the thermal regime of salt-marsh channel beds, *Environ. Sci. Technol.*, 42(3), 671–676.
- Neilson, B. T. (2006), Dynamic stream temperature modeling: Understanding the causes and effects of temperature impairments and uncertainty in predictions, Ph.D. dissertation, Utah State Univ., Logan.
- Sayde, C., C. Gregory, M. G. Rodriguez, N. Tuffillaro, S. Tyler, N. van de Giesen, M. English, R. Cuenca, and J. Selker (2010), Feasibility of soil moisture monitoring with heated fiber optics, *Water Resour. Res.*, 46, W06201, doi:10.1029/2009WR007846.
- Selker, J. S., L. Thevenaz, H. Huwald, M. Alfred, W. Luxemburg, N. van de Giesen, M. Stejskal, J. Zeman, M. Westhoff, and M. B. Parlange (2006a), Distributed fiber-optic temperature sensing for hydrologic systems, *Water Resour. Res.*, 42, W12202, doi:10.1029/2006WR005326.
- Selker, J. S., N. van de Giesen, M. Westhoff, W. Luxemburg, and M. B. Parlange (2006b), Fiber optics opens window on stream dynamics, *Geophys. Res. Lett.*, 33, L24401, doi:10.1029/2006GL027979.
- Sellers, W. D. (1965), *Physical Climatology*, Univ. of Chicago Press, Chicago, Ill.
- Sinokrot, B. A., and H. G. Stefan (1993), Stream temperature dynamics: Measurements and modeling, *Water Resour. Res.*, 29(7), 2299–2312.
- Steele-Dunne, S. C., M. M. Rutten, D. M. Krzeminska, M. Hausner, S. W. Tyler, J. Selker, T. A. Bogaard, and N. C. van de Giesen (2010), Feasibility of soil moisture estimation using passive distributed temperature sensing, *Water Resour. Res.*, 46, W03534, doi:10.1029/2009WR008272.
- Stonestrom, D. A., and J. Constantz (2003), *Heat as a tool for studying the movement of ground water near streams*, 96 pp., U.S. Geol. Surv., Denver, Colo.
- Sweeny, C., A. Gnanadesikan, S. M. Griffies, M. J. Harrison, A. J. Rosati, and B. L. Samuels (2005), Impacts of shortwave penetration depth on large-scale ocean circulation and heat transport, *J. Physical Oceanogr.*, 35, 1103–1119.
- Tyler, S. W., S. A. Burak, J. P. McNamara, A. Lamontagne, J. S. Selker, and J. Dozier (2008), Spatially distributed temperatures at the base of two mountain snowpacks measured with fiber optics sensors, *J. Glaciol.*, 54, 673–679.
- Tyler, S. W., J. S. Selker, M. B. Hausner, C. E. Hatch, T. Torgersen, C. E. Thodal, and G. Schladow (2009), Environmental temperature sensing using Raman spectra DTS fiber-optic methods, *Water Resour. Res.*, 45, W00D23, doi:10.1029/2008WR007052.
- Wang, J., and J. Seyed-Yagoobi (1994), Effects of water turbidity and salt concentration levels on penetration of solar radiation under water, *Sol. Energy*, 52(5), 429–438.
- Webb, B. W., and Y. Zhang (1997), Spatial and seasonal variability in the components of the river heat budget, *Hydrol. Processes*, 11(1), 79–101.
- Westhoff, M. C., H. H. G. Savenije, W. M. J. Luxemburg, G. S. Stelling, N. C. van de Giesen, J. S. Selker, L. Pfister, and S. Uhlenbrook (2007), A distributed stream temperature model using high resolution temperature observations, *Hydrol. Earth Syst. Sci.*, 11, 1469–1480.
- H. Ban, Mechanical and Aerospace Engineering, Utah State University, 4130 Old Main Hill, Logan, UT 84321, USA. (heng.ban@usu.edu)
- C. E. Hatch and S. W. Tyler, Department of Geological Sciences and Engineering, University of Nevada, Reno, MS172, Reno, NV 89557, USA.
- B. T. Neilson, Utah Water Research Laboratory, Civil and Environmental Engineering, Utah State University, 8200 Old Main Hill, Logan, UT 84321, USA. (bethany.neilson@usu.edu)